Journal of Biomolecular NMR, 6 (1995) 189–197
ESCOM

J-Bio NMR 281

A new triple-resonance experiment for the sequential assignment of backbone resonances in proteins

Frank Löhr and Heinz Rüterjans*

Institut für Biophysikalische Chemie, Johann Wolfgang Goethe Universität Frankfurt am Main, Biozentrum, Marie Curie Strasse 9, D-60439 Frankfurt am Main, Germany

Received 31 January 1995
Accepted 30 March 1995

Keywords: Triple-resonance NMR spectroscopy; Sequential assignment; Reduced dimensionality; *Desulfovibrio vulgaris* flavodoxin

Summary

A new protocol is described for obtaining intraresidual and sequential correlations between carbonyl carbons and amide ^{1}H and ^{15}N resonances of amino acids. Frequency labeling of ^{13}CO spins occurs during a period required for the $^{13}C^{\alpha}$-^{15}N polarization transfer, leading to an optimized transfer efficiency. In a four-dimensional version of the experiment, $^{13}C^{\alpha}$ chemical shifts are used to improve the dispersion of signals. The resonance frequencies of all backbone nuclei can be detected in a 3D variant in which cross peaks are split along two frequency axes. This pulse scheme is the equivalent of a five-dimensional experiment. The novel pulse sequences are applied to flavodoxin from *Desulfovibrio vulgaris*.

Introduction

The original set of triple-resonance experiments (Ikura et al., 1990; Kay et al., 1990) should in principle yield sufficient correlations for the assignment of all backbone resonances in isotopically enriched proteins. Only interresidual connectivities between carbonyl carbons and amide ^{1}H and ^{15}N nuclei are provided by the HNCO experiment. However, intraresidual correlations can only be obtained indirectly by a combination of the HNCA and HCACO experiments. Thus, ambiguities due to $^{13}C^{\alpha}$ chemical shift degeneracy are transferred to the assignment of ^{13}CO resonances and linkages between intra- and interresidual correlations are based solely on the information present in the HNCA spectrum. Further difficulties may arise from isotope shifts if the HCACO experiment is recorded using a sample in D_2O solution. These problems can be overcome with the HN(CA)CO experiment (Clubb et al., 1992) by making use of $^{1}J(C^{\alpha}N)$ and $^{2}J(C^{\alpha}N)$ couplings for intra- and interresidual correlations between ^{1}H, ^{15}N and ^{13}CO. A disadvantage of this method is the relatively low sensitivity compared to other triple-resonance experiments, so that usually only a relatively small fraction of the interresidual connectivities can be observed. We present here a new method which provides the same correlations as the HN(CA)CO experiment but with improved sensitivity, allowing for a sequential assignment by alignment of ^{13}CO resonances. In this experiment ^{13}CO chemical shifts are exploited as a way to establish connectivities between adjacent amide groups, independent of HNCA-type correlations. Furthermore, their assignment can be useful for a separation of side-chain CH cross peaks (Kay et al., 1992; Kay, 1993). Remaining overlap in the three-dimensional version can be resolved by detecting $^{13}C^{\alpha}$ chemical shifts in a fourth dimension. In cases where overlap in three dimensions is not a serious problem, the chemical shifts of all backbone nuclei can be obtained in a 3D version by applying the principle of dimensionality reduction (Szyperski et al., 1993a) twice.

A drawback of the HN(CA)CO experiment is the loss of observable magnetization due to an incomplete buildup of $^{13}C^{\alpha}$ antiphase magnetization with respect to ^{13}CO, and to the evolution of the passive $^{1}J(C^{\alpha}C^{\beta})$ coupling during the polarization transfer from α-carbons to carbonyl carbons. This could be circumvented by adjusting the duration of the $^{13}C^{\alpha}$ relay steps to $1/^{1}J(C^{\alpha}C^{\beta})$ (~27–28 ms). Transverse relaxation of $^{13}C^{\alpha}$, however, would then lead to a severe reduction in sensitivity, since this period appears

*To whom correspondence should be addressed.

A 3D (HCA)CO(CA)NH

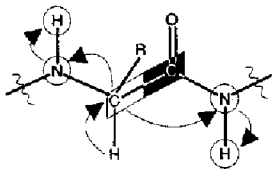

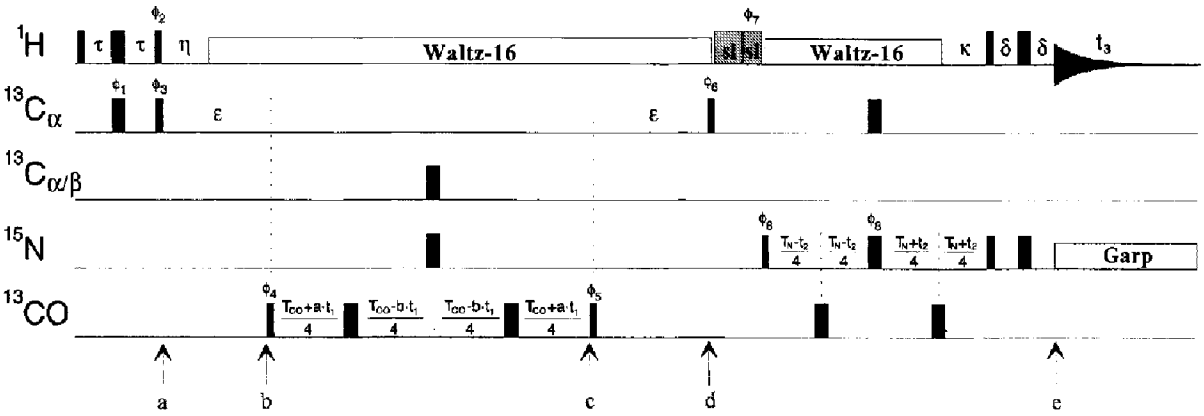

B 4D (H)CACOCANH

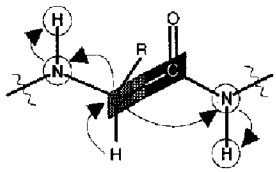

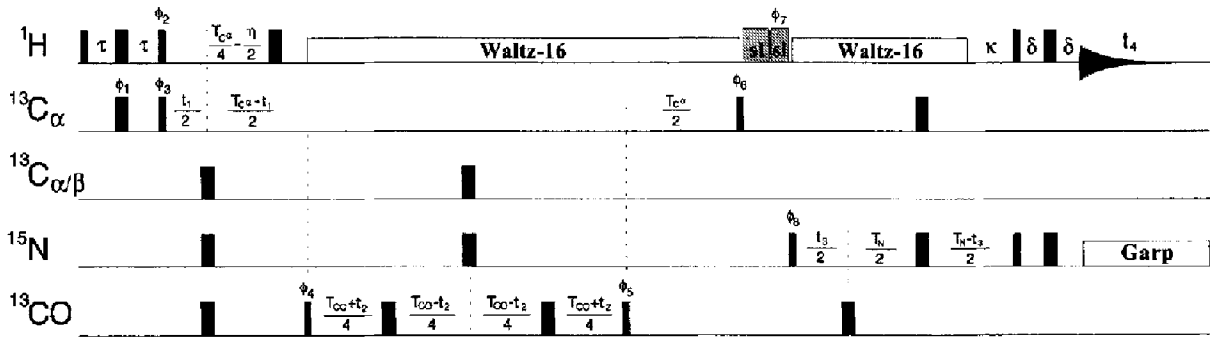

C 3D HCACOCANH

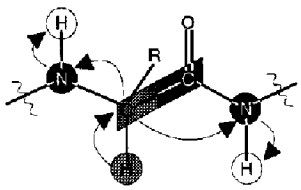

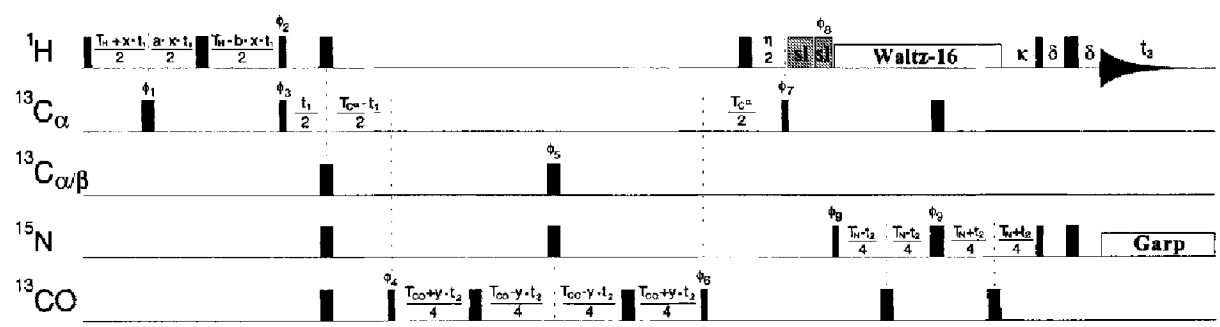

twice in the HN(CA)CO sequence. Recently we have proposed a modified HCACO experiment (Löhr and Rüterjans, 1995) where ^{13}CO chemical shifts are observed in a C^{α}-CO 'HMQC' manner. In this pulse sequence the total duration of $^{13}C^{\alpha}$ transverse magnetization is $1/^{1}J(C^{\alpha}C^{\beta})$ and the delays for de- and rephasing of $^{13}C^{\alpha}$ magnetization with respect to the coupled ^{13}CO spin are tuned to $1/[2\,^{1}J(C^{\alpha}C')]$, resulting in an optimized transfer efficiency. This protocol is employed for the correlation of carbonyl carbons with amide nitrogens and protons in the pulse sequences depicted in Fig. 1. The period of $^{13}C^{\alpha}$ transverse magnetization in which the correlation with ^{13}CO chemical shifts takes place can simultaneously be exploited for dephasing with respect to ^{15}N spins. Thus, it is appropriate to refrain from the 'out-and-back' concept and start with excitation of α-protons instead, leading to a shorter pulse sequence when compared to the HN(CA)CO scheme. The new pulse sequences, which we will refer to as HCACOCANH, essentially are combinations of a modified HCACO sequence with the HCANNH experiment (Montelione and Wagner, 1990; Kay et al., 1991; Boucher et al., 1992).

Methods

In the following, a brief description of the 3D (HCA)CO(CA)NH sequence, which correlates carbonyl carbons with amide ^{15}N and ^{1}H nuclei of the same and the sequentially following amino acid residue, will be given in terms of the product operator formalism (Sørensen et al., 1983), using the spin operators $\mathbf{H}^{\alpha}$, $\mathbf{C}^{\alpha}$, $\mathbf{C}'$, $\mathbf{N}$ and $\mathbf{H}^{N}$ for the magnetization components of the $^{1}H^{\alpha}$, $^{13}C^{\alpha}$, ^{13}CO, ^{15}N and $^{1}H^{N}$ nuclei, respectively. Nonrelevant ^{2}J and ^{3}J $^{1}H,^{1}H$, $^{1}H,^{13}C$ and $^{1}H,^{15}N$ scalar interactions, as well as relaxation effects, are not considered and only terms that result in observable magnetization during the detection period are retained. The initial INEPT transfer (Morris and Freeman, 1979) converts longitudinal alpha-proton magnetization ($\mathbf{H}_z^{\alpha}$) into antiphase $^{13}C^{\alpha}$ magnetization:

$$\sigma(a) = -2\mathbf{H}_z^{\alpha}\mathbf{C}_y^{\alpha} \sin(2\pi\,{}^{1}J_{C^{\alpha}H^{\alpha}}\tau) \qquad (1)$$

The constant multiplicative factor is close to 1 and will be omitted in the following. Temporarily neglecting $^{13}C^{\alpha},^{13}C^{\beta}$ and $^{13}C^{\alpha},^{15}N$ couplings, transverse $^{13}C^{\alpha}$ magnetization has become antiphase with respect to carbonyl carbons while it has been rephased with respect to protons at the end of the first delay ε:

$$\sigma(b) = -2\mathbf{C}_y^{\alpha}\mathbf{C}_z' \sin(\pi\,{}^{1}J_{C^{\alpha}H^{\alpha}}\eta)\cos^{n}(\pi\,{}^{1}J_{C^{\alpha}H^{\alpha}}\eta) \sin(\pi\,{}^{1}J_{C^{\alpha}C'}\varepsilon) \qquad (2)$$

The exponent n is 1 for glycine and zero for all other residues. The first 90° ^{13}CO pulse transfers this term into C^{α},CO two-spin coherence. During the subsequent constant-time period T_{CO}, carbonyl chemical shifts are allowed to evolve while those of α-carbons are refocused, yielding:

$$\sigma(c) = -2\mathbf{C}_y^{\alpha}\mathbf{C}_y' \sin(\pi\,{}^{1}J_{C^{\alpha}H^{\alpha}}\eta)\cos^{n}(\pi\,{}^{1}J_{C^{\alpha}H^{\alpha}}\eta) \sin(\pi\,{}^{1}J_{C^{\alpha}C'}\varepsilon)\cos(\Omega_{CO}t_1) \qquad (3)$$

where Ω_{CO} is the angular ^{13}CO frequency. Following the second 90° ^{13}CO pulse, rephasing of $\mathbf{C}_y^{\alpha}\mathbf{C}_z'$ transverse magnetization occurs according to:

$$\sigma(d) = \mathbf{C}_x^{\alpha}\sin(\pi\,{}^{1}J_{C^{\alpha}H^{\alpha}}\eta)\cos^{n}(\pi\,{}^{1}J_{C^{\alpha}H^{\alpha}}\eta) \sin^{2}(\pi\,{}^{1}J_{C^{\alpha}C'}\varepsilon)\cos(\Omega_{CO}t_1) \qquad (4a)$$

Homonuclear $^{13}C^{\alpha},^{13}C^{\beta}$ as well as one- and two-bond heteronuclear $^{13}C^{\alpha},^{15}N$ couplings are active throughout the period $2\varepsilon + T_{CO}$, whereas the $^{1}J(C'N)$ coupling is refocused during T_{CO}. Considering only intraresidual correlations,

←

Fig. 1. Pulse schemes of the HCACOCANH experiment. (A) Three-dimensional version; (B) four-dimensional version; (C) three-dimensional version with twofold reduced dimensionality. The insets show the magnetization transfer pathways, where the boxes mark the nuclei that are involved in two-spin coherence. Narrow and wide bars denote pulses with 90° and 180° flip angles, respectively. Positions of the ^{13}C carrier are 177.3 ppm (A), 60.1 ppm (B) and 170.0 ppm (C). Off-resonance square pulses on aliphatic carbons are centred at 58 ppm ($^{13}C^{\alpha}$) and 48 ppm ($^{13}C^{\alpha\beta}$), with their rf field strengths adjusted to provide a null in the excitation profile at the ^{13}CO region. Carbonyl 90° and 180° pulses are implemented as phase-modulated pulses with an amplitude profile corresponding to the central lobe of a sinc function and durations of 124 μs (600 MHz spectrometer) and 150 μs (500 MHz spectrometer). In all sequences the carbonyl pulses are applied at 177.3 ppm. In the first part of variants A and B, the proton carrier frequency is placed on the water resonance and at 6.4 ppm in the case of sequence C. It is moved to the centre of the amide region immediately before application of the first ^{15}N 90° pulse. A synchronous WALTZ-16 scheme (Shaka et al., 1983) with rf fields of 4.5 and 4.0 kHz is used for proton decoupling at 600 and 500 MHz, respectively. Water suppression is accomplished by a pair of orthogonal spin-lock purge pulses (sl) applied for 3 and 2 ms, and for pulse sequences B and C additionally by weak (5 Hz field) presaturation. GARP-1 modulation (Shaka et al., 1985) with field strengths of 0.9 and 0.8 kHz are employed for ^{15}N decoupling during acquisition at a 600 and a 500 MHz spectrometer, respectively. Delay durations and phase cycles are as follows: (A) $\tau = 1.7$ ms, $\eta = 2.4$ ms, $\varepsilon = 8$ ms, $T_{CO} = 11$ ms, $a = 1.54$, $b = 0.46$, $T_N = 22$ ms, $\kappa = 5.4$ ms, $\delta = 2.3$ ms, $\phi_1 = x,-x$, $\phi_2 = y,-y$, $\phi_3 = 2(x),2(-x)$, $\phi_4 = 4(x),4(-x)$, $\phi_5 = x+45°$, $\phi_6 = x+67°$, $\phi_7 = y$, $\phi_8 = 8(x),8(-x)$, Rec.: $+,-,-,+,-,+,+,-,-,+,+,-,+,-,-,+$; (B) $\tau = 1.7$ ms, $T_{C\alpha} = 18$ ms, $\eta = 2.4$ ms, $T_{CO} = 9$ ms, $T_N = 22$ ms, $\kappa = 5.4$ ms, $\delta = 2.3$ ms, $\phi_1 = x,-x$, $\phi_2 = y,-y$, $\phi_3 = 2(x)$, $2(-x)$, $\phi_4 = 4(x),4(-x)$, $\phi_5 = x+80°$, $\phi_6 = x-45°$, $\phi_7 = y$, $\phi_8 = 8(x),8(-x)$, Rec.: $+,-,-,+,-,+,+,-,-,+,+,-,-,+,-,+$; (C) $T^{H} = 3.5$ ms, $a = 0.58$, $b = 0.42$, $x = 0.625$, $T_{C\alpha} = 18$ ms, $T_{CO} = 11$ ms, $y = 0.2$, $\eta = 2.2$ ms. $T_N = 22$ ms, $\kappa = 5.4$ ms, $\delta = 2.3$ ms, $\phi_1 = x,-x$, $\phi_2 = y,-y$, $\phi_3 = 2(x),2(-x)$, $\phi_4 = 4(x),4(-x)$, $\phi_5 = (16x),16(-x)$, $\phi_6 = \phi_7 = x+70°$, $\phi_8 = y$, $\phi_9 = 8(x),8(-x)$, Rec.: $+,-,-,+,-,+,+,-,-,+,+,-,+,-,-,+$. Non-labeled pulses are applied along the x-axis. The phases of the pulses labeled ϕ_5 and ϕ_6 in sequences A and B and of the pulses labeled ϕ_6 and ϕ_7 in sequence C are adjusted to compensate for Bloch–Siegert phase errors as indicated. Quadrature detection in the indirectly sampled dimensions is achieved by altering the phases ϕ_4 (t_1) and ϕ_8 (t_2) in sequence A, ϕ_3 (t_1), ϕ_4 (t_2) and ϕ_8 (t_3) in sequence B, and ϕ_3 (t_1) and ϕ_9 (t_2) in sequence C in the States-TPPI manner (Marion et al., 1989).

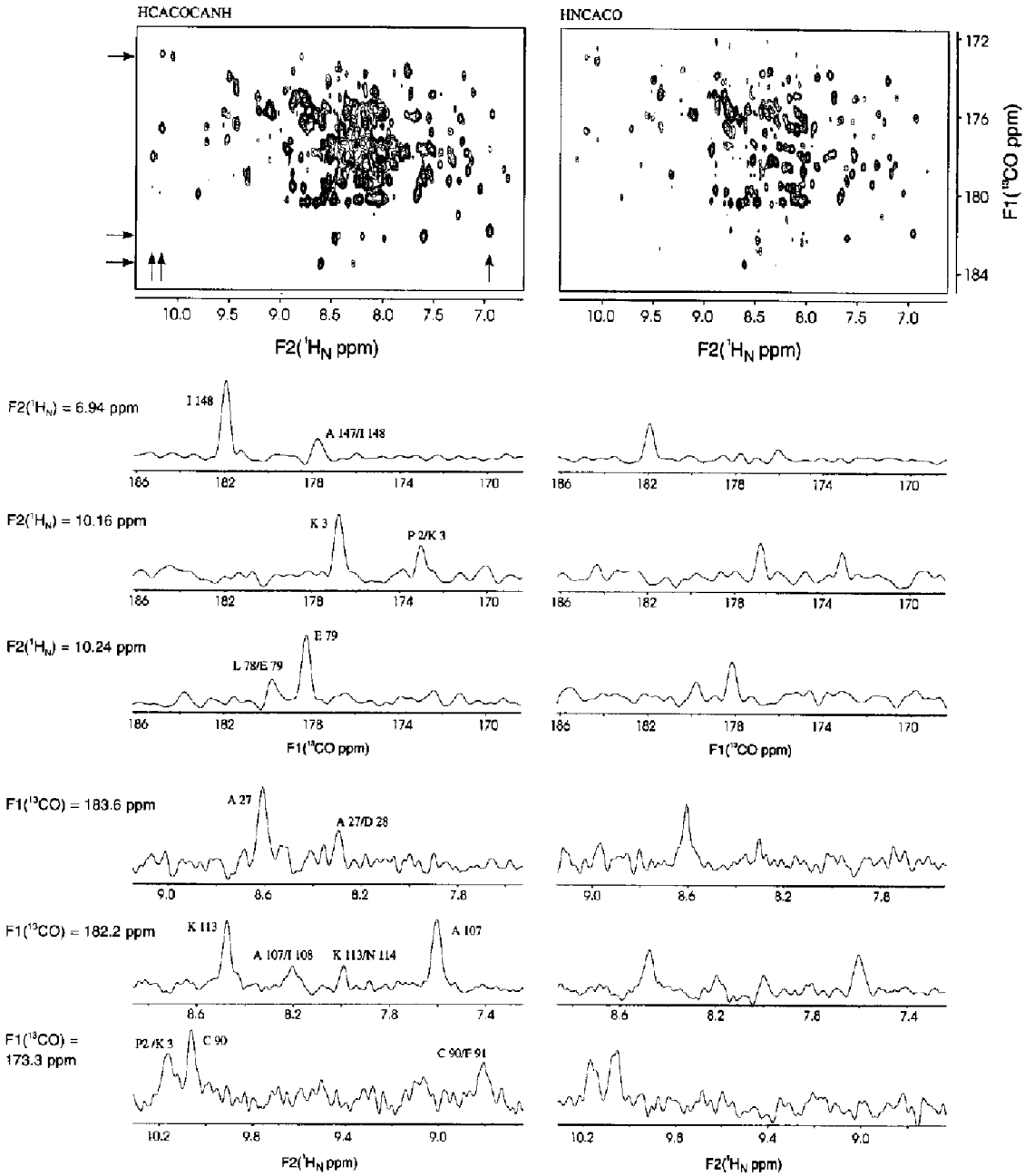

Fig. 2. Two-dimensional (HCA)CO(CAN)H (left) and H(NCA)CO (right) spectra of *D. vulgaris* flavodoxin, recorded under identical experimental conditions on a Bruker DMX-500 spectrometer. Acquisition times were 19.7 ms in t_1 and 106.7 ms in t_2. The measuring time for each of the 44×512 complex data sets was 32 min, accumulating 16 scans per FID. Positive and negative contour lines are drawn without distinction. The heights of the contour levels are chosen equal for the two spectra, using a spacing factor of $2^{1/2}$. F1 and F2 traces are taken at the positions indicated by the arrows. The cross sections are plotted at the same noise level within each pair belonging to a particular F1 or F2 position.

these effects are summarized by:

$$\begin{aligned}\sigma(\mathrm{d}) = 2\mathbf{C}_y^{\alpha}\mathbf{N}_z \sin(\pi\,{}^1J_{C\alpha H\alpha}\eta)\cos^n(\pi\,{}^1J_{C\alpha H\alpha}\eta)\\ \sin^2(\pi\,{}^1J_{C\alpha C'}\varepsilon)\sin[\pi\,{}^1J_{C\alpha N}(2\varepsilon + T_{CO})]\\ \cos[\pi\,{}^2J_{C\alpha N}(2\varepsilon + T_{CO})]\\ \cos[\pi\,{}^1J_{C\alpha C\beta}(2\varepsilon + T_{CO})]\cos(\Omega_{CO}t_1)\end{aligned} \quad (4b)$$

The pair of 90° $^{13}C^{\alpha}/^{15}N$ pulses, separated by two proton spin-lock purge pulses, converts the $^{13}C^{\alpha}$ antiphase magnetization into ^{15}N antiphase magnetization which is refocused with respect to α-carbons during the subsequent ^{15}N constant-time chemical shift evolution period. Finally, a reverse INEPT sequence creates observable magnetization of amide protons described by Eq. 5:

$$\begin{aligned}\sigma(\mathrm{e}) = \mathbf{H}_x^N \sin(\pi\,{}^1J_{C\alpha H\alpha}\eta)\cos^n(\pi\,{}^1J_{C\alpha H\alpha}\eta)\\ \sin^2(\pi\,{}^1J_{C\alpha C'}\varepsilon)\sin[\pi\,{}^1J_{C\alpha N}(2\varepsilon + T_{CO})]\\ \cos[\pi\,{}^2J_{C\alpha N}(2\varepsilon + T_{CO})]\cos[\pi\,{}^1J_{C\alpha C\beta}(2\varepsilon + T_{CO})]\\ \sin(\pi\,{}^1J_{C\alpha N}T_N)\cos(\pi\,{}^2J_{C\alpha N}T_N)\\ \cos(\Omega_{CO}t_1)\cos(\Omega_N t_2)\end{aligned} \quad (5)$$

where incomplete de- and rephasing of ^{15}N and $^{1}H^{N}$ transverse magnetization in the last polarization transfer step is neglected. An almost identical expression is obtained for the interresidual correlations, the only difference being the mutual exchange of sine and cosine functions in the terms with the $^{1}J(C^{\alpha}N)$ and $^{2}J(C^{\alpha}N)$ couplings.

The signal amplitude of the HCACOCANH experiment can be optimized by adjusting the delays ε and T_{CO} to $1/[2\,^{1}J(C^{\alpha}CO)]$ and $[1/^{1}J(C^{\alpha}C^{\beta})]-2\varepsilon$, respectively, i.e., any reduction associated with the evolution of active and passive carbon–carbon couplings is avoided. The disadvantage of an extended period of $^{13}C^{\alpha}$ transverse magnetization when compared to the HN(CA)CO experiment is partially compensated by the reduced overall duration of the HCACOCANH pulse sequence and the smaller number of pulses. In the latter sequence, the duration for which the magnetization resides on $^{13}C^{\alpha}$ is prolonged by approximately 14 ms, but a 25 ms period of ^{15}N transverse magnetization has been saved. Assuming a C^{α}-CO transfer efficiency of 1 for the HCACOCANH and $\cos^2(\pi\,^{1}J(C^{\alpha}C^{\beta})\Delta)\times\sin^2[\pi\,^{1}J(C^{\alpha}CO)\Delta]=0.45$ ($\Delta=7$ ms, $^{1}J(C^{\alpha}C^{\beta})=35$ Hz, $^{1}J(C^{\alpha}CO)=55$ Hz), the theoretical ratio of sensitivities for a medium-sized protein can be calculated to be 1.66, using T_2 values of 28 and 120 ms for $^{13}C^{\alpha}$ and ^{15}N, respectively. For larger proteins (MW > 30 kDa) with transverse relaxation times around 16 ms ($^{13}C^{\alpha}$) and 70 ms (^{15}N), the theoretical sensitivity gain in favour of the HCACOCANH experiment is 1.32, implying that the method proposed here might still be useful in the resonance assignment process in cases where the HN(CA)CO experiment fails.

Experimental

The various versions of the HCACOCANH sequence are demonstrated on a 2.2 mM sample of uniformly ^{13}C, ^{15}N-labeled *Desulfovibrio vulgaris* flavodoxin (147 amino acids) in its oxidized state (Knauf et al., 1993).The protein was dissolved in 0.5 ml 10 mM potassium phosphate buffer, pH 7, containing 5% D_2O. Processing of 3D spectra was performed using the TRITON software, while the 4D data set was processed with the FELIX 1.1 program. The 3D (HCA)CO(CA)NH spectrum was acquired at 27 °C on a Bruker AMX-600 spectrometer equipped with a multichannel interface and a triple-resonance $^{1}H/^{13}C/^{15}N$ probe. Spectral widths were 2128, 1488 and 4808 Hz in F1, F2 and F3, respectively. The spectrum was recorded as a 48 (complex) × 32 (complex) × 1024 (real) points data set, corresponding to acquisition times of 22.9 ms (t_1), 20.8 ms (t_2) and 106.5 ms (t_3). Time-domain data were extended to 56 and 42 points in t_1 and t_2 by linear prediction. The size of the absorptive part of the 3D spectrum was 128 × 64 × 1024. The total measuring time, using 16 scans per FID, was 36 h.

The 4D (H)CACOCANH was recorded at 600 MHz as an 18 (complex) × 14 (complex) × 8 (complex) × 512 (real) points data set, with acquisition times of 5.6, 6.7, 4.7 and 59 ms in t_1, t_2, t_3 and t_4, respectively. Spectral widths covered 3012 Hz in F1, 1932 Hz in F2, 1488 Hz in F3 and 4348 Hz in F4. In the F2 (^{13}CO) domain, resonances are folded nine times because the carbon carrier frequency was not switched to the carbonyl region prior to the ^{13}CO evolution time. A frequency jump would have resulted in a loss of phase coherence on our spectrometer. The measuring time, using 16 transients per FID, was 79.5 h. After Fourier transformation in the ^{15}N and $^{1}H^{N}$ dimensions, time-domain data were extended to 26 points in t_1 and 22 points in t_2 and Fourier transformed as well. Then, inverse Fourier transformation,

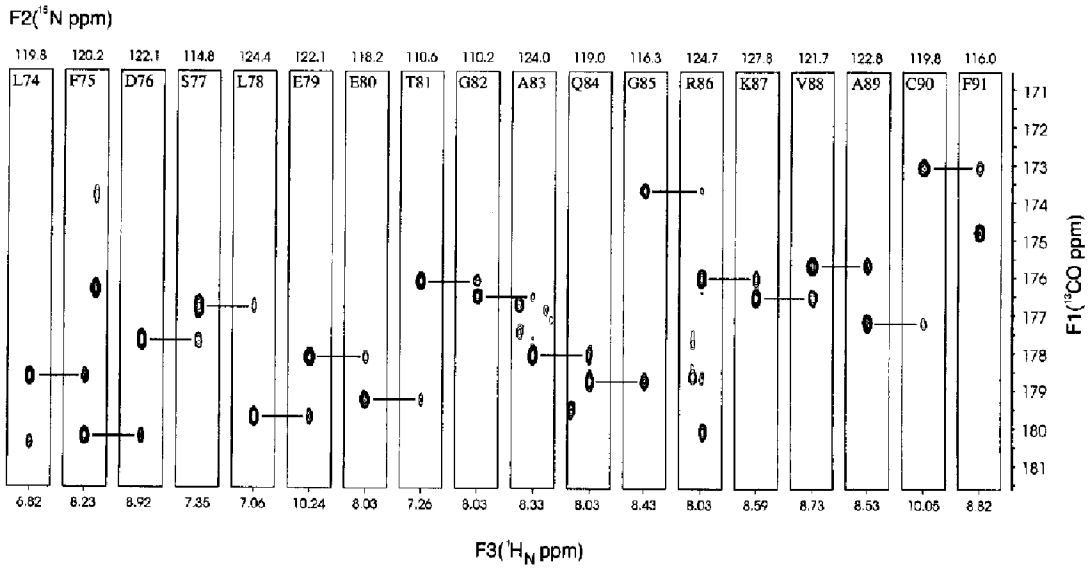

Fig. 3. Sequential assignment of residues Leu^{74}–Phe^{91} of oxidized *D. vulgaris* flavodoxin from a 3D (HCA)CO(CA)NH spectrum. The ^{13}CO (F1), $^{1}H^{N}$ (F3) strips are taken at the ^{15}N (F2) chemical shifts indicated at the top of each panel. Cross peaks at the ^{13}CO chemical shifts of glycine residues have a negative sign due to the $^{13}C^{\alpha}$ transverse magnetization period of $1/^{1}J(C^{\alpha}C^{\beta})$. Sequential connectivities are indicated by horizontal lines.

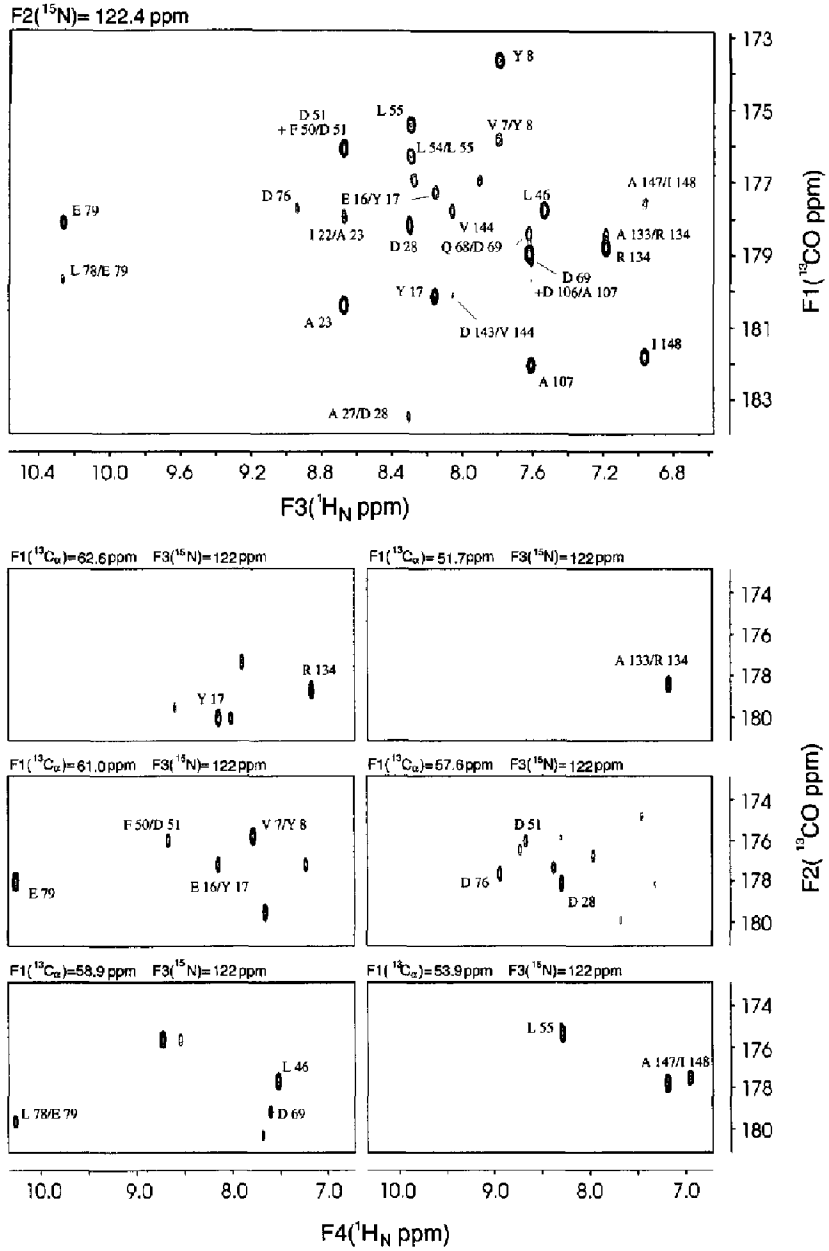

Fig. 4. Top: F1,F3-slice from the 3D (HCA)CO(CA)NH spectrum of *D. vulgaris* flavodoxin. Bottom: selected F2,F4-slices from the 4D (H)CACOCANH spectrum taken at the F3 (^{15}N) chemical shift that is nearest to the F2 (^{15}N) position of the plane at the top. Unlabeled cross peaks are due to the poorer digital resolution in the ^{15}N dimension of the 4D spectrum and appear in adjacent slices of the 3D spectrum.

linear prediction yielding 14 complex points, and Fourier transformation was applied to the F3 dimension. The final size of the 4D matrix was $64\times64\times32\times512$ real points.

The 3D HCACOCANH spectrum was recorded on a Bruker DMX-500 spectrometer equipped with three channels and a triple-resonance probe tuned to ^{1}H, ^{13}C and ^{15}N. For each FID of 512 complex points, 32 scans were accumulated and 64 (t_1) $\times$ 32 (t_2) complex increments were collected, resulting in a measuring time of 88.5 h. Spectral widths in the $^{1}H^{\alpha}$, $^{13}C^{\alpha}$, ^{13}CO, ^{15}N and $^{1}H^{N}$ domains comprised 7542, 4712, 8562, 1712 and 3501 Hz, respectively. Resonances were folded three times in the $^{13}C^{\alpha}$ domain, such that the centre of the spectral region corresponded to 57.5 ppm. Acquisition times were 8.4 ms (t_1, $^{1}H^{\alpha}$), 13.5 ms (t_1, $^{13}C^{\alpha}$), 3.9 ms (t_2, ^{13}CO), 19.8 ms (t_2, ^{15}N) and 73.4 ms (t_3, $^{1}H^{N}$). The transfer time of the initial INEPT step was incorporated into the $^{1}H^{\alpha}$ evolution period in a semi-constant-time manner. Thus, the apparent relaxation rate and the passive proton–proton J-couplings were scaled down with a factor $[t_1\,(^{1}H^{\alpha})_{max} - T^{H}]/t_1\,(^{1}H^{\alpha})_{max}$ in the t_1 dimension (Grzesiek and Bax, 1993). Linear prediction was applied to extend the time-domain data to 80 and 44 complex points in t_1 and t_2, respectively. The size of the absorptive part of the 3D spectrum was $256\times128\times512$ points.

Results and Discussion

The superior sensitivity of the HCACOCANH experiment is verified experimentally in Fig. 2, which shows 2D $^{1}H^{N}$,^{13}CO correlation maps obtained with the pulse sequence of Fig. 1A and the sequence described by Clubb et al. (1992). These two-dimensional spectra correspond to the first point in the ^{15}N time domain of the respective 3D versions. In order to ensure a fair comparison, the original HN(CA)CO pulse scheme was slightly modified. The following changes have been made: (i) the periods in which ^{15}N magnetization rephases with respect to $^{1}H^{N}$ and dephases with respect to $^{13}C^{\alpha}$ and vice versa were concatenated, such that four 180° pulses and two 5.4 ms delay durations could be saved; (ii) during the time that the magnetization is on the ^{15}N nuclei, the offset for proton decoupling was centered in the amide region; and (iii) spin-lock pulses for water suppression were implemented in the same way as in the HCACOCANH pulse sequences of Fig. 1. Clearly, the intensity of nearly all cross peaks, excluding those for glycine residues, is considerably higher in the (HCA)CO(CAN)H spectrum. Several correlations can be identified that do not emerge from the noise level in the H(NCA)CO spectrum. One-dimensional cross sections through well-resolved cross peaks are shown at the bottom of Fig. 2. The gain in the S/N ratio observed for the (HCA)CO(CAN)H in comparison to the H(NCA)CO spectrum ranged from 1.1 to 2.0. The largest value was found for the C-terminal amino acid (Ile^{148}), indicating a relatively long T_2 ($^{13}C^{\alpha}$) time due to its increased mobility.

For simplicity, the evaluation of the sensitivity as well as the product operator description are given for a constant-time version (a = b = 1) in which the ^{13}CO chemical shift evolution time will be limited to approximately 10 ms. In order to improve the experimental resolution, the carbonyl evolution period has to be implemented in a semi-constant-time manner (Grzesiek and Bax, 1993; Logan et al., 1993) with $1 < a < 2$ and $b = 2 - a$. Note that in this case modulations with $^{1}J(C^{\alpha}C^{\beta})$, $^{1}J(C^{\alpha}N)$ and $^{2}J(C^{\alpha}N)$ scaled down with a factor of $a - 1$ ($= (a - b)/2$) will be imposed on the ^{13}CO dimension.

The (HCA)CO(CA)NH experiment provides a means for the sequential assignment of backbone resonances in analogy to the HNCA experiment, i.e., pairs of ^{13}CO chemical shifts are linked by common correlations to amide proton and nitrogen chemical shifts. This is demonstrated in Fig. 3 for residues Leu^{74} to Phe^{91} of *D. vulgaris* flavodoxin. The relatively high sensitivity of this experiment permits the identification of all intraresidual and sequential cross peaks. Even for glycine residues (e.g. Gly^{82}, Gly^{85}) these correlations are still present, although the signal amplitudes are attenuated by the passive $^{1}J(H^{\alpha}C^{\alpha})$ coupling in the refocused INEPT step at the beginning of the pulse sequence. In other cases, the identification of sequential connectivities for flavodoxin was prevented by overlap. This problem can easily be circumvented by introducing a fourth dimension, yielding a better dispersion and more information for the process of resonance assignment. In the four-dimensional version of the HCACOCANH experiment (Fig. 1B), constant-time $^{13}C^{\alpha}$ chemical shift evolution is achieved by simultaneously moving 180° pulses on $^{13}C^{\alpha/\beta}$, ^{13}CO and ^{15}N through the first ε period of the 3D (HCA)CO(CA)NH. Since α-carbons and carbonyl carbons are correlated in an 'HMQC' manner, both the delays for the buildup and the refocusing of $^{13}C^{\alpha}$ antiphase magnetization with respect to ^{13}CO spins can be exploited for chemical shift evolution of α-carbons (Madsen and Sørensen, 1992), allowing for a maximal evolution time of $1/^{1}J(C^{\alpha}CO) \sim 18$ ms. Although this feature is not of any significance for the 4D (H)CACOCANH experiment due to the limited number of increments, it could be useful in a 3D (H)CACOCA(N)H version which would supply the same correlations as the H(N)CACO pulse sequence (Seip et al., 1993), with improved resolution in the $^{13}C^{\alpha}$ domain.

Figure 4 shows one of the most crowded F1,F3-slices from the 3D (HCA)CO(CA)NH and several F2,F4-slices from the 4D (H)CACOCANH spectrum, taken at approximately the same ^{15}N chemical shift as the plane from the three-dimensional spectrum. Any overlap present in the three-dimensional (HCA)CO(CA)NH spectrum of flavodoxin was completely removed in its four-dimension-

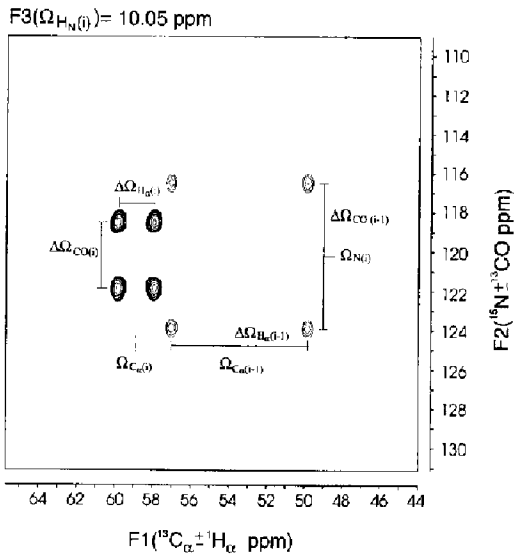

Fig. 5. Expansion of an F1,F2-slice of the HCACOCANH spectrum obtained with the pulse sequence from Fig. 1C. The intraresidual correlation for Cys^{90} (residue i) of *D. vulgaris* flavodoxin and the sequential Ala^{89}/Cys^{90} correlation are shown. The midpoints of the rectangles appear at the ^{15}N chemical shift of Cys^{90} and the $^{13}C^{\alpha}$ chemical shifts of Cys^{90} and Ala^{89}, which can be read directly from the scales at the F1 and F2 axes. $^{1}H^{\alpha}$ and ^{13}CO chemical shifts are obtained from the splittings along the two indirectly detected dimensions. The splittings (in Hz) are scaled down using the factors x = 0.625 and y = 0.2, such that 1 ppm splitting in F1 corresponds to $\Delta\Omega(H^{\alpha}) = 0.2$ ppm and 1 ppm splitting in F2 corresponds to $\Delta\Omega(CO) = 1$ ppm.

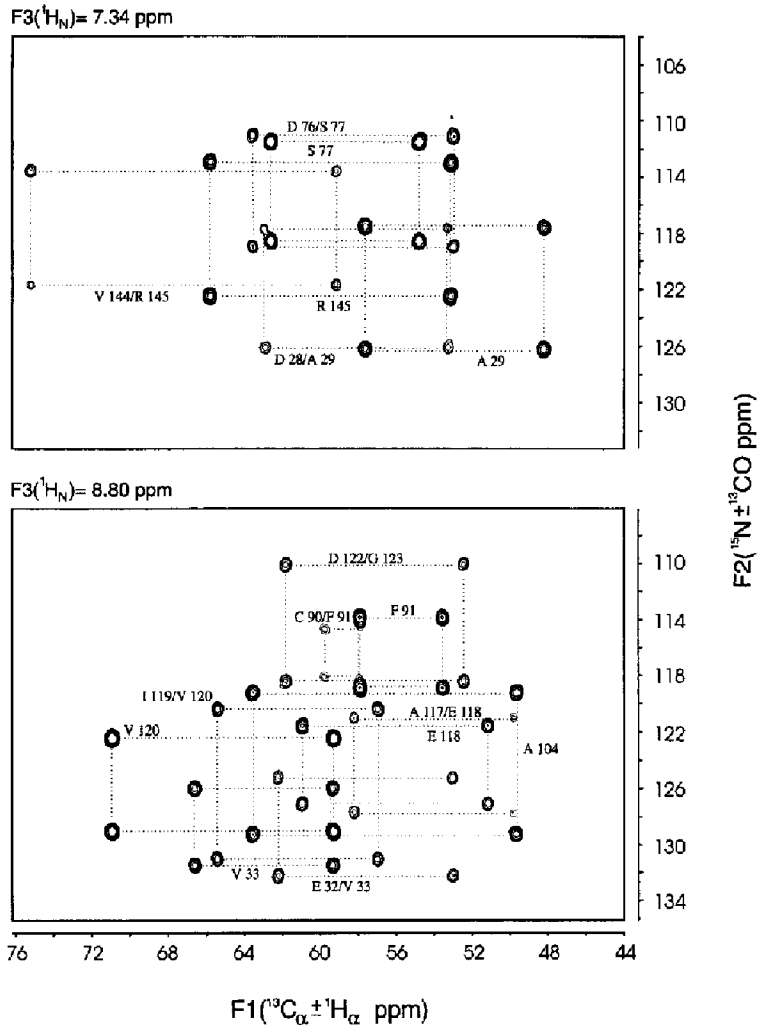

Fig. 6. Representative F1,F2 planes from the HCACOCANH spectrum of flavodoxin with twofold reduced dimensionality. For clarity, the four cross-peak components belonging to each intraresidual and sequential correlation are connected by broken lines. Since only positive levels were plotted, the intraresidual signals for Gly[123] cannot be seen here.

al version. For example, the sequential connectivities between residues Phe[50] and Asp[51] and between Ala[133] and Arg[134] could not be identified unambiguously from the 3D spectrum, due to the degeneracy of the ^{13}CO resonances within the sequential pairs. In contrast, the intra- and interresidual cross peaks are resolved in the 4D spectrum by their different chemical shifts in the F1 ($^{13}C^{\alpha}$) dimension.

Recently it has been shown by Szyperski et al. (1993a, b,1994) and by Simorre et al. (1994) that the chemical shift information of 4D and 3D triple-resonance experiments can be preserved in three-dimensional and two-dimensional variants, respectively. This is achieved by simultaneously incrementing two evolution periods while applying quadrature detection only to one nucleus. Failure of discriminating between positive and negative frequencies for the second species leads to a splitting of the cross peaks, from which the offset from the carrier can be determined. Since the HCACOCANH experiment potentially comprises five frequency domains, the principle of dimensionality reduction can be employed twice, leading to the pulse sequence of Fig. 1C, where chemical shift evolution of four different nuclei is monitored in two indirect dimensions. The resonance frequencies of $^{1}H^{\alpha}$ and $^{13}C^{\alpha}$ can be observed in F1 and those of ^{13}CO and ^{15}N in F2. Quadrature detection is applied to the $^{13}C^{\alpha}$ and ^{15}N domains, such that signals appear at the sum and the difference of $^{13}C^{\alpha}$ and $^{1}H^{\alpha}$ chemical shifts in F1 and at the sum and the difference of ^{15}N and ^{13}CO chemical shifts in F2. As depicted in Fig. 5, the resulting cross peaks consist of four components, arranged in a rectangular pattern in the planes perpendicular to the acquisition domain F3. The position of the centre along F1 and F2 is determined by the $^{13}C^{\alpha}$ and ^{15}N chemical shifts, while the distances between the components reflect the $^{1}H^{\alpha}$ and ^{13}CO offsets from the respective carrier frequencies, which were placed at the edges of the spectral regions (6.4 ppm for $^{1}H^{\alpha}$ and 170 ppm for ^{13}CO). To simplify the extraction of $^{1}H^{\alpha}$ and ^{13}CO resonance frequencies, the scaling factors $x = \Delta t_1$ ($^{1}H^{\alpha}$) / Δt_1 ($^{13}C^{\alpha}$) and $y = \Delta t_2$ (^{13}CO) / Δt_2 (^{15}N) were introduced in a way that the splittings still have a suitable size.

The distribution of signal intensity on four cross-peak components in the 3D HCACOCANH version leads to a theoretical reduction of the signal-to-noise ratio by a factor of two when compared to the five-dimensional experiment from which it is derived. However, as pointed out by Simorre et al. (1994) for the case of two-dimensional versions of the HNCA and HNCO experiments, the identification of a pair of signals with known symmetry properties is easier than the identification of a single peak at the same signal-to-noise ratio. This advantage should be even more significant for patterns of four signals that result from the pulse scheme described here. More important is that a 3D spectrum can of course be obtained with a much better digital resolution and less demanding data handling and processing than the corresponding 5D spectrum recorded within the same measuring time. Figure 6 shows two typical examples for F1,F2-slices of a 3D HCACOCANH spectrum. Despite the relatively large number of signals, it was not difficult to identify the components that belong to the individual correlations and overlap appears not to be a serious problem for a protein the size of flavodoxin. Sequential connectivities within the planes can be detected by the common F2 positions of the midpoints of the intra- and interresidual rectangular patterns. Thus, in principle, the complete sequential assignment of all backbone ^{1}H, ^{13}C and ^{15}N resonances can be achieved with a single 3D experiment.

Conclusions

An efficient experiment has been presented which provides intra- as well as interresidual carbonyl-to-amide correlations in proteins. The 3D (HCA)CO(CA)NH sequence can be used to resolve ambiguities in the standard set of spectra in which the detection of sequential connectivities relies on common correlations to α-carbons. For flavodoxin, the three versions of the new experiment revealed all expected intra- and interresidual correlations, with the exception of a few cases in the 3D (HCA)CO-(CA)NH and 3D HCACOCANH spectra, where cross peaks were obscured by overlap. In favourable cases, the total number of experiments for the backbone resonance assignment might be reduced with the help of 4D (H)CA-COCANH or 3D HCACOCANH spectra.

Acknowledgements

The help of Prof. Stephen Mayhew (Department of Biochemistry, University College Dublin) and Dr. Martin Knauf in labeling and isolation of the *D. vulgaris* flavodoxin is gratefully acknowledged.

References

Boucher, W., Laue, E.D., Campbell-Burk, S.L. and Domaille, P.J. (1992) *J. Biomol. NMR*, **2**, 631–637.

Clubb, R.T., Thanabal, V. and Wagner, G. (1992) *J. Magn. Reson.*, **97**, 213–217.

Grzesiek, S. and Bax, A. (1993) *J. Biomol. NMR*, **3**, 185–204.

Ikura, M., Kay, L.E. and Bax, A. (1990) *Biochemistry*, **29**, 4659–4667.

Kay, L.E., Ikura, M., Tschudin, R. and Bax, A. (1990) *J. Magn. Reson.*, **89**, 496–514.

Kay, L.E., Ikura, M. and Bax, A. (1991) *J. Magn. Reson.*, **91**, 84–92.

Kay, L.E., Ikura, M., Grey, A.A. and Muhandiram, D.R. (1992) *J. Magn. Reson.*, **99**, 652–659.

Kay, L.E. (1993) *J. Am. Chem. Soc.*, **115**, 2055–2057.

Knauf, M., Löhr, F., Curley, G.P., O'Farrell, P., Mayhew, S.G., Müller, F. and Rüterjans, H. (1993) *Eur. J. Biochem.*, **213**, 167–184.

Logan, T.M., Olejniczak, E.T., Xu, R.X. and Fesik, S.W. (1993) *J. Biomol. NMR*, **3**, 225–231.

Löhr, F. and Rüterjans, H. (1995) *J. Magn. Reson.*, manuscript submitted for publication.

Madsen, J.C. and Sørensen, O.W. (1992) *J. Magn. Reson.*, **100**, 431–436.

Marion, D., Ikura, M., Tschudin, R. and Bax, A. (1989) *J. Magn. Reson.*, **85**, 393–399.

Montelione, G.T. and Wagner, G. (1990) *J. Magn. Reson.*, **87**, 183–188.

Morris, G.A. and Freeman, R.J. (1979) *J. Am. Chem. Soc.*, **101**, 760–762.

Seip, S., Balbach, J. and Kessler, H. (1993) *J. Biomol. NMR*, **3**, 233–237.

Shaka, A.J., Keeler, J., Frenkiel, T. and Freeman, R. (1983) *J. Magn. Reson.*, **52**, 335–338.

Shaka, A.J., Barker, P.B. and Freeman, R. (1985) *J. Magn. Reson.*, **64**, 547–552.

Simorre, J.-P., Brutscher, B., Caffrey, M.S. and Marion, D. (1994) *J. Biomol. NMR*, **4**, 325–333.

Sørensen, O.W., Eich, G.W., Levitt, M.H., Bodenhausen, G. and Ernst, R.R. (1983) *Prog. NMR Spectrosc.*, **16**, 163–192.

Szyperski, T., Wider, G., Bushweller, J.H. and Wüthrich, K. (1993a) *J. Biomol. NMR*, **3**, 127–132.

Szyperski, T., Wider, G., Bushweller, J.H. and Wüthrich, K. (1993b) *J. Am. Chem. Soc.*, **115**, 9307–9308.

Szyperski, T., Pellechia, M. and Wüthrich, K. (1994) *J. Magn. Reson. Ser. B*, **105**, 188–191.